applied sciences

MDPI

Communication

Fractional Sliding Mode Harmonic Control of an Active Power Filter

Wesley Fei [1,2] and Mingang Hua [1,*]

[1] College of IoT Engineering, Hohai University, Changzhou 213022, China; wesleyfei1@163.com
[2] Changzhou Senior High School of Jiangsu Province, Changzhou 213004, China
* Correspondence: mg.hua@hotmail.com

Abstract: A sliding mode control (SMC) strategy with a fractional-order scheme is developed to provide an effective way to compensate for the harmonic current and strengthen the performance of an active power filter (APF). The formulation of a fractional-order sliding mode controller (FOSMC) is incorporated in the current control of an APF control system, obtaining an extra degree of freedom over integer-order ones to improve the dynamic property. The simulation results of the APF utilizing the designed strategy confirm the satisfactory performance and smaller total harmonic distortion (THD) by comparative study.

Keywords: fractional sliding mode controller; harmonic compensation; active power filter

check for updates

Citation: Fei, W.; Hua, M. Fractional Sliding Mode Harmonic Control of an Active Power Filter. *Appl. Sci.* **2023**, *13*, 3815. https://doi.org/10.3390/app13063815

Academic Editor: Sergio Toscani

Received: 2 February 2023
Revised: 14 March 2023
Accepted: 14 March 2023
Published: 16 March 2023

Copyright: © 2023 by the authors. Licensee MDPI, Basel, Switzerland. This article is an open access article distributed under the terms and conditions of the Creative Commons Attribution (CC BY) license (https://creativecommons.org/licenses/by/4.0/).

1. Introduction

Today, in addition to the wide application of power electronic equipment and frequency conversion technology, new energy power generation is developing rapidly to improve energy quality. As a result, the nonlinear loads in the power grid have become more complex, which introduces challenges to the safe and stable operation of the power grid [1–3]. In recent years, with the development of the new energy industry, the importance of harmonic suppression has been emphasized. For example, both grid-connected wind and photovoltaic power systems are equipped with nonlinear power electronic devices, which produce certain harmonic and DC components. When the harmonic is injected into the power system, it causes the distortion of the voltage and current, which triggers the power system's relay protection and the misoperation of automatic devices, affecting the safe operation of the power system [4–6].

Therefore, it is urgent to deal with harmonics in a power grid. The common solutions are harmonic prevention and harmonic compensation. Harmonic compensation only requires a parallel or series compensation device on the load side. An active power filter (APF) has the advantages of great flexibility, excellent compensation, and superior controllability and has become the main equipment for harmonic compensation. The traditional harmonic current compensation tracking control is not good enough to give full play to the superior characteristics of the APF. The control strategy of the compensation current is the key point to the compensation capability of APF. Therefore, many studies have been carried out on the compensation current control strategy. At present, various control strategies, such as a neural network algorithm [7], fuzzy control [8], sliding mode control [9,10], repetitive control [11–13], feedback linearization [14], digital control [15], model predictive control [16,17], backstepping control [18], etc., have been proposed and have proved effective in numerous fields of industrial production.

Sliding mode control (SMC) is a type of discontinuous nonlinear control with high robustness, which is usually used to deal with uncertainties and disturbances in the system [19–22]. Since the advantage of sliding mode control is its robustness to external disturbances as well as changes and uncertainties in the internal parameters, it is very suitable for APF current control, which is difficult to model and requires high control

accuracy. However, sliding mode control has a chattering problem. Therefore, over the years, some sliding mode controllers have been proposed to improve their performance. Fractional calculus is a form of research dating back centuries; the fractional-order integrator and differentiator can provide an extra degree of freedom to design a controller, and transfer energy more slowly than that of an integer-order counterpart, attenuating chattering [23–25]. Ghasemi et al. [26] presented a robust controller with fractional calculus for wind turbine generators. Cao et al. [27] found that a fractional adaptive fuzzy controller had better dynamic properties than integer ones. Ullah et al. [28] presented a new adaptive FOSMC for a permanent magnet synchronous motor.

Motivated by the above literature, an FOSMC for a three-phase APF is developed to achieve good working performance. The FOSMC has fast convergence and a small steady-state error in the phase of sliding mode. The contributions of this paper are as follows:

(1) A novel sliding mode control method combining a fractional-order method and sliding mode control is proposed in this paper. It not only has the characteristics of a small tracking error and reduced chattering but also ensures the tracking error converges fast.
(2) This paper extends integer-order SMC to fractional ones. It is a challenge to combine the SMC together with fractional-order control and apply these to the three-phase APF. An FOSMC has more degrees of freedom to obtain the desired performance. The key property of the method is to select the order of the fractional module and choose suitable parameters to achieve the best performance.
(3) A simulation study further proves the good performance in eliminating the harmonic current while stabilizing the DC side voltage. Meanwhile, the superiority of the proposed control scheme was verified through detailed comparisons and analysis.

The rest of this paper is organized as follows. In Section 2, a dynamic model of APF is established. In Section 3, a fractional-order SMC method is proposed and analyzed. Simulation studies are given in Section 4. Eventually, Section 5 gives the conclusions.

2. Dynamic Model of an Active Power Filter

As shown in Figure 1, an APF consists of three parts, a harmonic current detection module, a current tracking control module, and a generating circuit of compensation current. A harmonic current detection module usually utilizes the rapid detection of harmonic currents, which is based on instantaneous reactive power theory. The compensation current of a three-phase three-wire APF is produced by a pulse width modulation (PWM) signal generator under normal circumstances. In order to achieve the purpose of eliminating the harmonic components of the current, the compensating current should be generated with the absolutely opposite phase and amplitude to that of the harmonic current. By collecting the current and voltage signals of the circuit from the sensor, the controller of the APF can output corresponding control signals, which will be modulated into a PWM wave. The PWM wave will then be sent to the insulated gate bipolar transistor (IGBT) driver to determine the states of the IGBT and generate the compensation current injected into the circuit, whose amplitude is equal to but sign is opposite to the harmonic current.

The basic operating principle of an APF is to detect the voltage and current produced by the operating system. The harmonic current detection is based on the Synchronous Reference Frame (SRF). After being calculated by the current operation circuit, the command signal i_c^* of the compensating current is obtained. With the aim of achieving the compensating current i_c, the signal which is produced by the PWM needs to be enlarged by amplifiers due to its small amplitude. Only when the compensating current offsets the harmonic current can we obtain the expected source current.

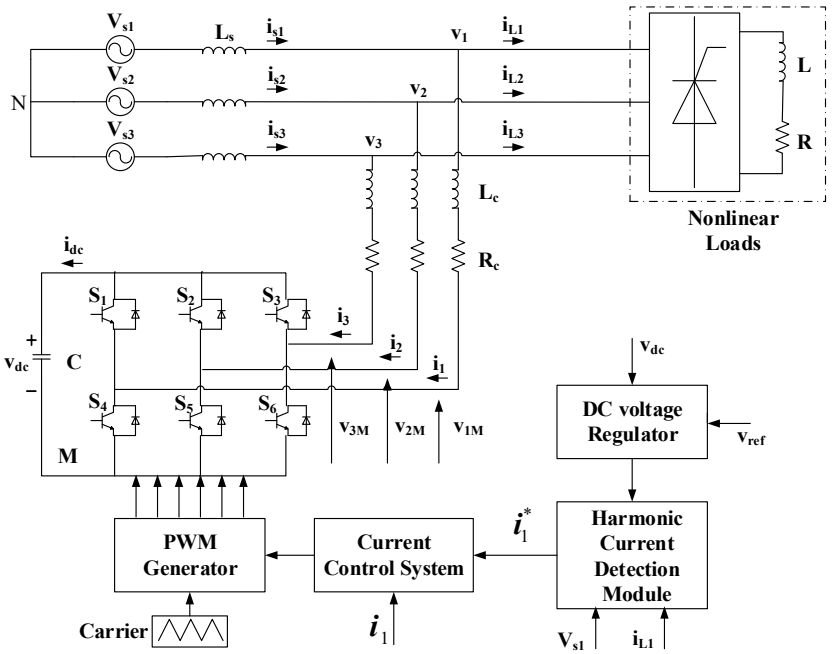


Figure 1. Block diagram of the main circuit of an APF.

Then, a dynamic model of the APF is developed. According to the circuit structure of an APF, applying Kirchhoff rules to the circuitry, we obtain:

$$\begin{cases} v_1 = L_c \dfrac{di_1}{dt} + R_c i_1 + v_{1M} + v_{MN} \\ v_2 = L_c \dfrac{di_2}{dt} + R_c i_2 + v_{2M} + v_{MN} \\ v_3 = L_c \dfrac{di_3}{dt} + R_c i_3 + v_{3M} + v_{MN} \end{cases}. \tag{1}$$

In the equations, L_c and R_c are the inductance and resistance, and ν_{MN} is the voltage from point M to N.

It is assumed the AC supply voltage is stable. Taking the Equations in (1) and combining with the absence of the zero-sequence in three wire system currents yields:

$$v_{MN} = -\frac{1}{3}\sum_{m=1}^{3} v_{mM} \tag{2}$$

By indicating the ON/OFF status of the IGBT, the switch function c_k becomes:

$$c_k = \begin{cases} 1, \text{ if } S_k \text{ is on and } S_{k+3} \text{ is off} \\ 0, \text{ if } S_k \text{ is off and } S_{k+3} \text{ is on} \end{cases}, \tag{3}$$

where $k = 1, 2, 3$.

At the same time, taking $v_{km} = c_k v_{dc}$ into consideration, (1) can be reformulated as:

$$\begin{cases} \dfrac{di_1}{dt} = -\dfrac{R_c}{L_c} i_1 + \dfrac{v_1}{L_c} - \dfrac{v_{dc}}{L_c}(c_1 - \dfrac{1}{3}\sum\limits_{m=1}^{3} c_m) \\ \dfrac{di_2}{dt} = -\dfrac{R_c}{L_c} i_2 + \dfrac{v_2}{L_c} - \dfrac{v_{dc}}{L_c}(c_2 - \dfrac{1}{3}\sum\limits_{m=1}^{3} c_m) \\ \dfrac{di_3}{dt} = -\dfrac{R_c}{L_c} i_3 + \dfrac{v_3}{L_c} - \dfrac{v_{dc}}{L_c}(c_3 - \dfrac{1}{3}\sum\limits_{m=1}^{3} c_m) \end{cases} \tag{4}$$

We define the switching state function as

$$d_{nk} = \left(c_k - \frac{1}{3} \sum_{m=1}^{3} c_m \right)_n \tag{5}$$

Equation (5) denotes the relationship between d_{nk} and c_k. Based on (5) and the eight permissible switching states of the IGBT, the following equation is obtained

$$\begin{bmatrix} d_{n1} \\ d_{n2} \\ d_{n3} \end{bmatrix} = \frac{1}{3} \begin{bmatrix} 2 & -1 & -1 \\ -1 & 2 & -1 \\ -1 & -1 & 2 \end{bmatrix} \begin{bmatrix} c_1 \\ c_2 \\ c_3 \end{bmatrix}. \tag{6}$$

Then, (4) is simplified as

$$\begin{cases} \frac{di_1}{dt} = -\frac{R_c}{L_c} i_1 + \frac{v_1}{L_c} - \frac{v_{dc}}{L_c} d_{n1} \\ \frac{di_2}{dt} = -\frac{R_c}{L_c} i_2 + \frac{v_2}{L_c} - \frac{v_{dc}}{L_c} d_{n2} \\ \frac{di_3}{dt} = -\frac{R_c}{L_c} i_3 + \frac{v_3}{L_c} - \frac{v_{dc}}{L_c} d_{n3} \end{cases}. \tag{7}$$

We define two state variables

$$x = i = (i_1 \quad i_2 \quad i_3)^T,\ \dot{x} = \dot{i},\ x = (x_{11} \quad x_{12} \quad x_{13})^T,\ \dot{x} = (x_{21} \quad x_{22} \quad x_{23})^T.$$

Taking the time derivative with respect to time yields

$$\begin{aligned} \dot{x}_k &= -\frac{R_c}{L_c} \dot{i}_k + \frac{1}{L_c} \frac{dv_k}{dt} - \frac{1}{L_c} \frac{dv_{dc}}{dt} d_{nk} \\ &= \frac{R_c^2}{L_c^2} i_k - \frac{R_c}{L_c^2} v_k + \frac{1}{L_c} \frac{dv_k}{dt} + (\frac{R_c}{L_c^2} v_{dc} - \frac{1}{L_c} \frac{dv_{dc}}{dt}) d_{nk} \end{aligned}, \tag{8}$$

where $k = 1, 2, 3$.

Considering the external disturbances, the model of an active power filter can be rewritten as

$$\dot{x} = f(x) + bu + d, \tag{9}$$

where $f(x_{1k}) = f(i_k) = \frac{R_c^2}{L_c^2} i_k - \frac{R_c}{L_c^2} v_k + \frac{1}{L_c} \frac{dv_k}{dt}$, $b = \frac{R_c}{L_c^2} v_{dc} - \frac{1}{L_c} \frac{dv_{dc}}{dt}$

$$u = d_n = (d_{n_1} \quad d_{n_2} \quad d_{n_3})^T,\ d = diag(d_1 \quad d_2 \quad d_3).$$

Assumption 1. *d is an unknown disturbance satisfying the condition $\rho - |d| > \sigma_1$. where ρ is a positive constant, and σ_1 is a tiny positive constant.*

3. Design of the Fractional Sliding Mode Control

3.1. Definitions of Fractional Derivatives and Integrals

We define ${}_aD_t^\alpha$ as a generalization of a differential and integral operator, where a and t are the bounds of the operation, and α is the order of fractional calculus. The commonly used three definitions are the Grunwald–Letnikov (GL) definition ${}_aD_t^\alpha f(t) = \lim_{h \to 0} h^{-\alpha} \sum_{j=0}^{\infty} (-1)^j \binom{\alpha}{j} (t - jh)$, the Riemann–Liouville (RL) definition,

${}_aD_t^\alpha f(t) = \frac{1}{\Gamma(n-\alpha)} \int_a^t \frac{f^{(n)}(\tau)}{(t-\tau)^{\alpha-n+1}} d\tau$ $n-1 < \alpha < n$, and the Caputo (C) definition.

In order to simplify the notation, the fractional derivative of order α is expressed as D^{α} instead of ${}_aD_t^{\alpha}$, defined as the Caputo definitionas

$$aD_t^{\alpha}f(t) = \begin{cases} \dfrac{1}{\Gamma(n-\alpha)}\int_a^t \dfrac{f^{(n)}(\tau)}{(t-\tau)^{\alpha-n+1}}d\tau, & n-1<\alpha<n \\ \dfrac{d^n}{dt^n}f(t), \alpha = n \end{cases}$$

where $f(\cdot)$ should be integrable, n is a positive integer, and $\Gamma(\cdot)$ represents the Gamma function as $\Gamma(n-\alpha) = \int_0^{\infty}\tau^{n-\alpha-1}e^{-\tau}d\tau$. The characteristic curve of the FOSMC and integer-order SMC are given in Figure 2, where the expression of the FOSMC close to equilibrium is $t^{-\alpha}$ after arriving at the sliding manifold, and the expression of the integer-order SMC is e^{-t}. It is obvious the chattering under the FO-SMC(Δ) is less than that of the integer-order SMC (Δ').

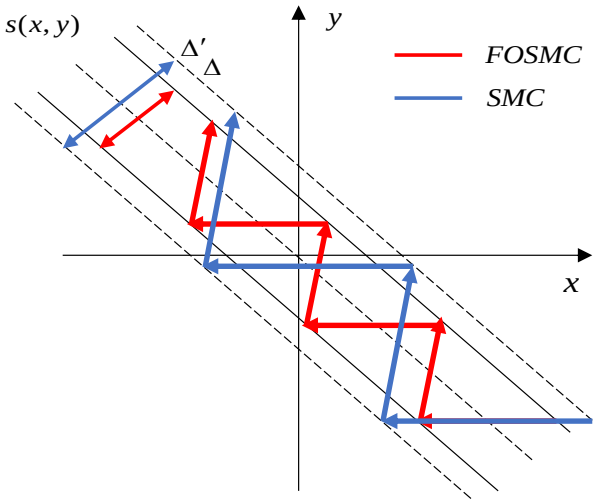


Figure 2. System properties under the FOSMC and SMC.

3.2. Fractional Sliding Mode Controller

Here, the design of the FOSMC is developed in detail, including how to improve the controller and certify the stable performance of the system. The block diagram of the FOSMC for an APF is shown in Figure 3. The intention is for current x to track a given reference current x_d.

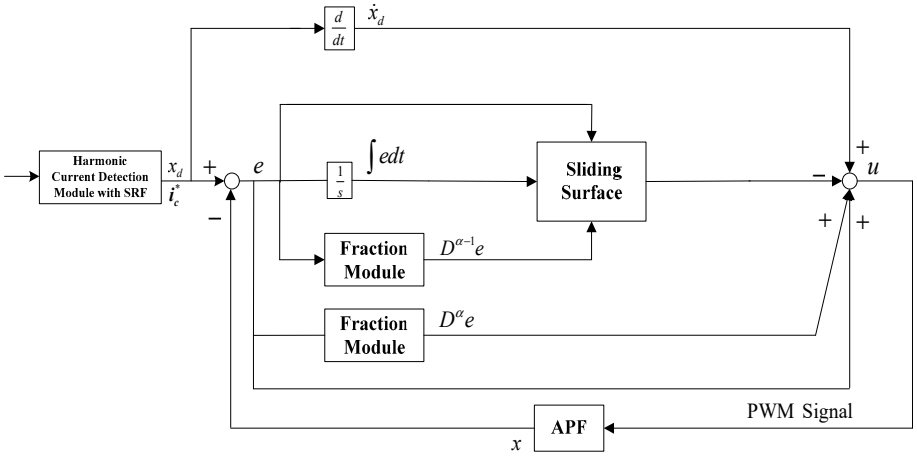


Figure 3. Block diagram of the FOSMC for an APF.

The tracking error is defined as

$$e = x_d - x \tag{10}$$

Then the derivative of Equation (10) is:

$$\dot{e} = \dot{x}_d - \dot{x}. \tag{11}$$

A fractional-order sliding mode surface is designed as

$$s = -\lambda_1 e - \lambda_2 \int e - \lambda_3 D^{\alpha-1} e \tag{12}$$

where $\lambda_1, \lambda_2, \lambda_3$ are positive and constant parameters. $\alpha - 1$ is the fractional order.

We differentiate the sliding surface:

$$\dot{s} = -\lambda_1 \dot{e} - \lambda_2 e - \lambda_3 D^{\alpha} e. \tag{13}$$

Then, substituting (11) into (13) yields

$$\dot{s} = -\lambda_1 \left(\dot{x}_d - f(x) - bu - d\right) - \lambda_2 e - \lambda_3 D^{\alpha} e. \tag{14}$$

Setting $\dot{s} = 0$ obtains the equivalent controller as

$$u_{eq} = \frac{1}{b\lambda_1}[-\lambda_1 f(x) - \lambda_1 d + \lambda_1 \dot{x}_d + \lambda_2 e + \lambda_3 D^{\alpha} e]. \tag{15}$$

Then, a controller is designed as

$$u = \frac{1}{b\lambda_1}\left[-\lambda_1 f(x) - \lambda_1 \rho \,\mathrm{sgn}\,(s) + \lambda_1 \dot{x}_d + \lambda_2 e + \lambda_3 D^{\alpha} e\right], \tag{16}$$

where $u_{sw} = -\lambda_1 \rho \mathrm{sgn}(s)$ is the switching function.

We choose a Lyapunov function as

$$V = \frac{1}{2} s^T s. \tag{17}$$

Differentiating (17) with respect to time yields

$$\dot{V} = s^T(-\lambda_1(\dot{x}_d - f(x) - bu - d) - \lambda_2 e - \lambda_3 D^{\alpha} e). \tag{18}$$

Substituting (16) into (18) yields

$$\begin{array}{l} \dot{V} = s^T(-\lambda_1[\dot{x}_d - f(x) - b\frac{1}{b\lambda_1}(-\lambda_1 f(x) - \lambda_1 \rho \mathrm{sgn}(s) + \lambda_1 \dot{x}_d + \lambda_2 e + \\ \lambda_3 D^{\alpha} e) - d] - \lambda_2 e - \lambda_3 D^{\alpha} e) \\ = s^T \lambda_1 (d - \rho \mathrm{sgn}(s)) \\ \leq \left|s^T\right| \lambda_1 (|d| - \rho). \end{array} \tag{19}$$

According to the Assumption, $\rho - |d| > \sigma_1$ and $\lambda_1 > 0$, thus $\dot{V} < 0$. This indicates that $s(t)$ is bounded. From (18), $\dot{s}(t)$ is bounded, showing $s(t)$ is uniformly continuous. According to the Barbalart lemma, $s(t)$ will asymptotically converge to zero, $\lim_{t\to\infty} s(t) = 0$ and $\lim_{t\to\infty} e(t) = 0$.

4. Simulation

The performance of the proposed FOSMC was evaluated on the platform of the Matlab/Simulink package with the SimPower Toolbox. A comparison between the fractional module controller and integer controller was also implemented. The parameters of the

APF control system are shown in Table 1. In the FOSMC, $\lambda_1 = 12, \lambda_2 = 3, \lambda_3 = 3$, and $\rho = 180000$. The APF starts to work at the time $t = 0.04$ s after switching on the compensation circuit. After implementing the FOSMC, it was obvious that the harmonics in the gird were efficiently offset, and the source current tended to a steady state after a half cycle, as shown in Figure 4. We demonstrated that the proposed FOSMC applied to an APF eliminated the harmonic current.

Table 1. Main parameters.

Supply Voltage and Frequency	$V_{s1} = V_{s2} = V_{s3} = 220$ V, $f = 50$ Hz
Switching frequency	$f_{sw} = 10$ KHz
The nonlinear load	$R = 10\ \Omega$, $L = 2$ mH
APF parameters	$L = 10$ mH, $C = 100$ μF $v_{dcref} = 1000$ V
PI controller	$k_p = 0.05$, $k_i = 0.01$

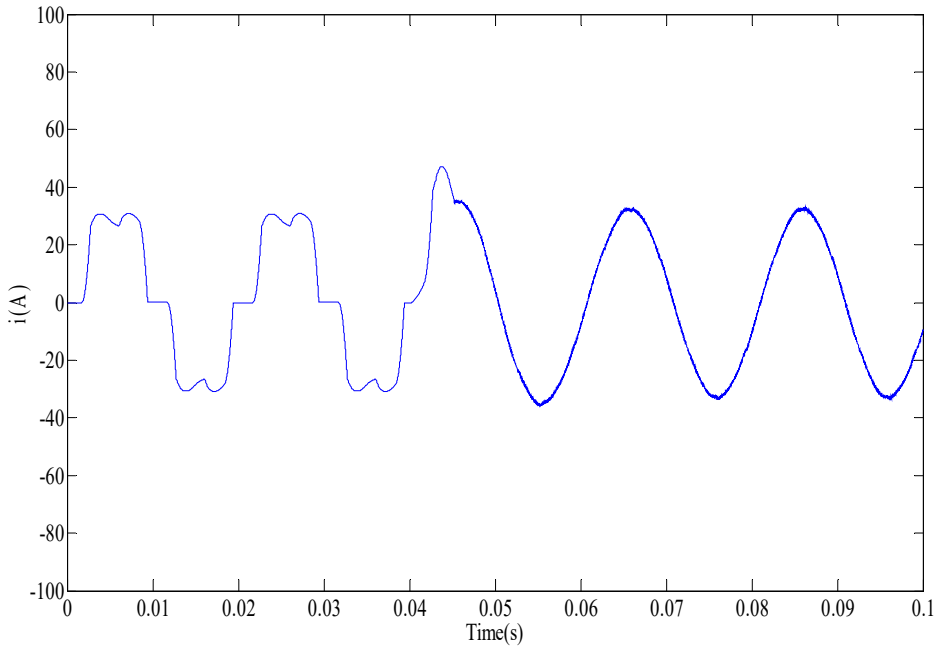
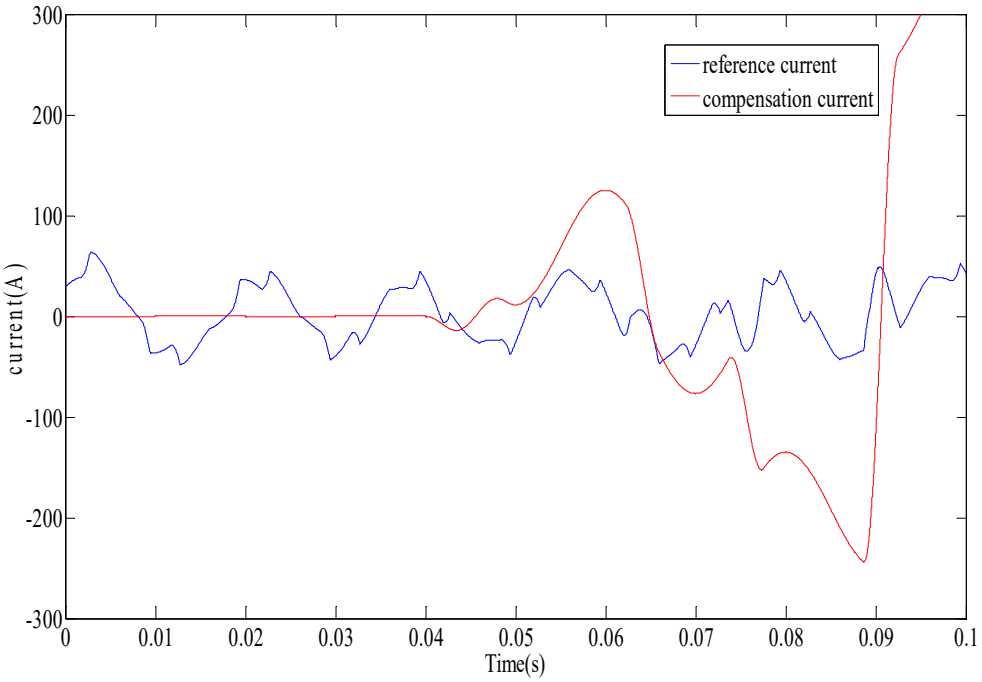
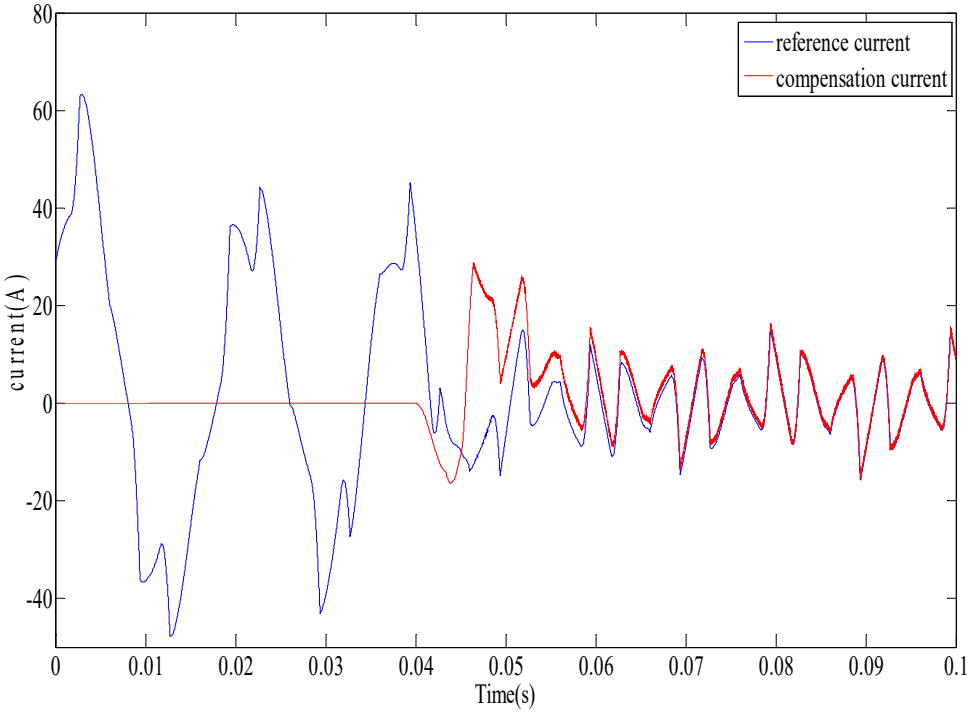


Figure 4. Improved source current of the A phase.

In order to achieve the best working performance in tracking the instruction current, Figure 5 gives different values of the fractional order. With the increasing values of the fraction order, the results became better. When α was too low ($\alpha = 0.2$), the compensation current could not quite track the instruction current. When $\alpha = 0.6$, the tracking trajectory was greatly improved, but it seemed inefficient for the length of the tracking time spent. When $\alpha = 0.9$, the result showed that after about 0.01 s, the compensation current could almost track the given instruction current. Then, in the simulation, α was chosen as $\alpha = 0.9$ in order to achieve satisfactory effects. The compensation tracking error is also given in Figure 6, confirming the effectiveness of the proposed FOSMC in the tracking function with a negligible error. Figure 7 further shows the good robustness for the quickly adjustable DC capacitor voltage, when the loads increased. Figure 8 shows the unqualified THD at the start of simulation. In Figure 9, after the APF worked, the THD was 1.55%, which was far less than the harmonic standard of the IEEE of 5%.

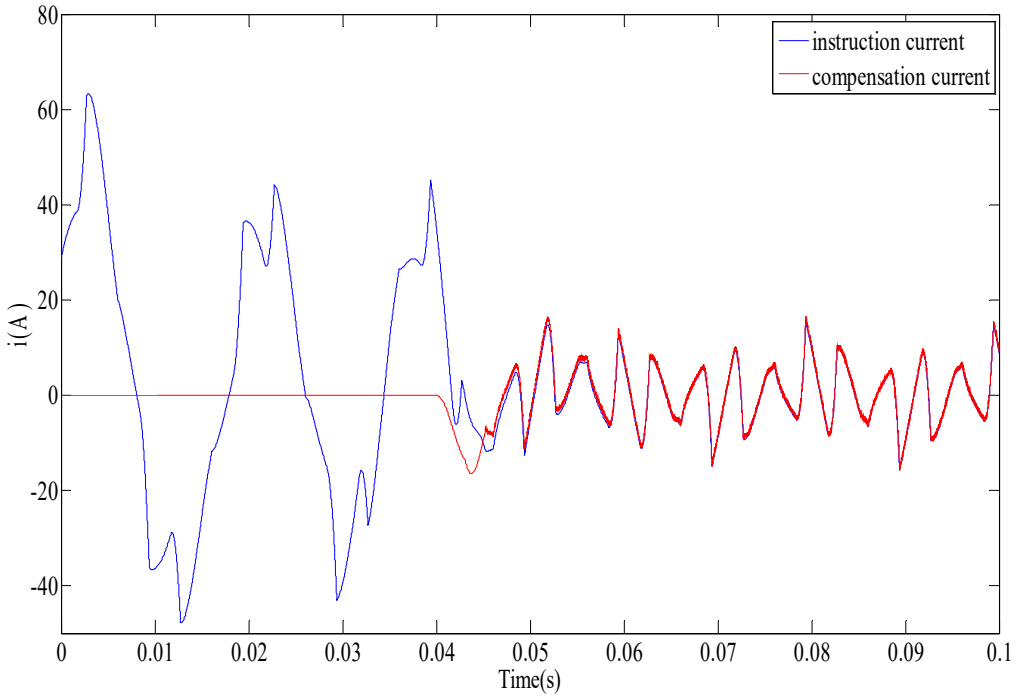


(**a**) $\alpha = 0.2$



(**b**) $\alpha = 0.6$

Figure 5. *Cont.*



(**c**) $\alpha = 0.9$

Figure 5. Instruction current and compensation current with different values of the fractional order.

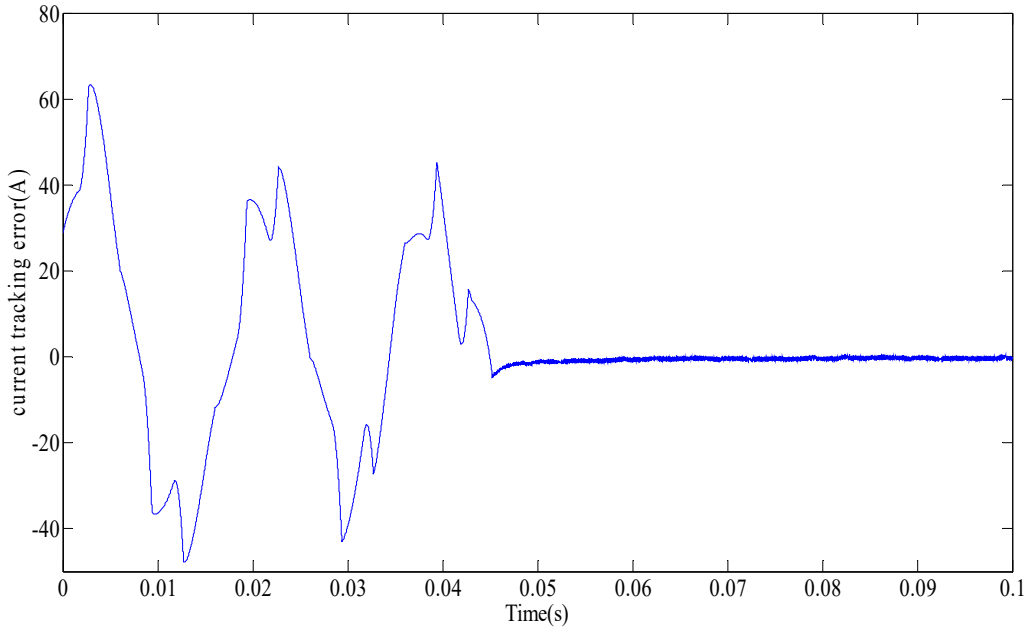


Figure 6. Compensation current tracking error.

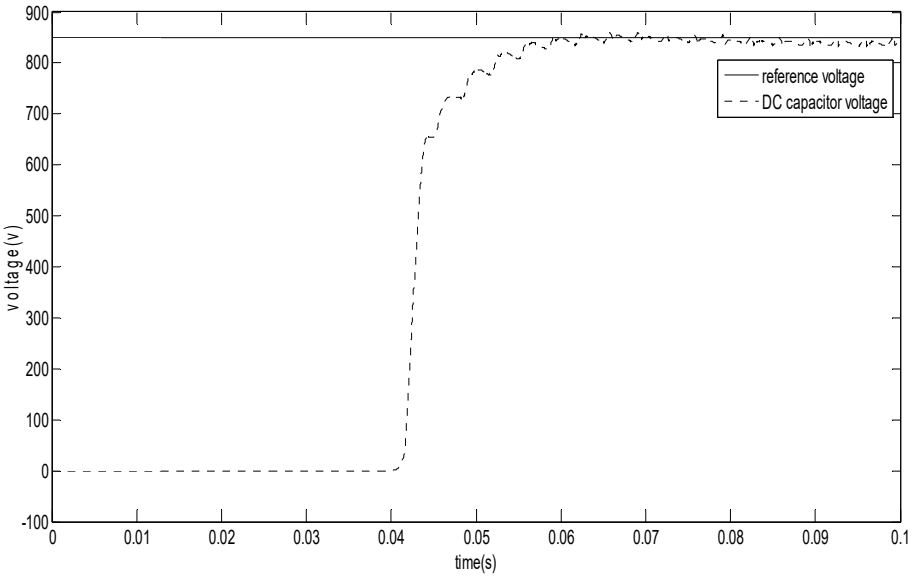


Figure 7. DC capacitor voltage without an increasing load.

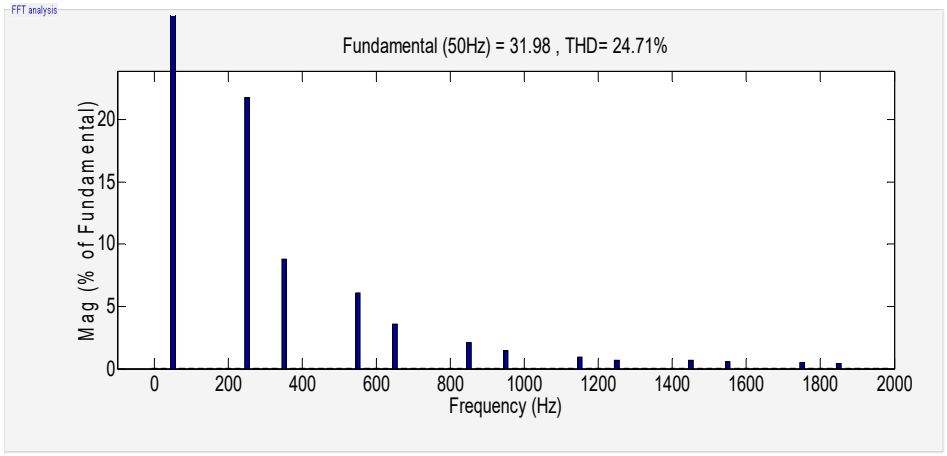


Figure 8. Harmonic spectrum of the source current at 0 s.

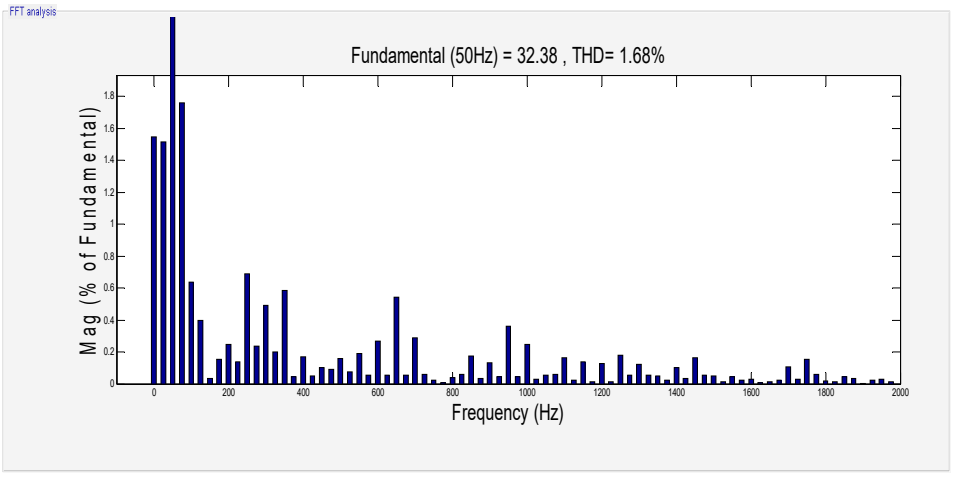


Figure 9. Harmonic spectrum of the source current at 0.06 s.

For the purpose of demonstrating that the fractional sliding mode control had good robustness in the presence of load changes, we added the loads in a ladder-type increase.

We added the same loads at the time of 0.1 s and 0.2 s in order to make sure that the applied loads increased. In Figures 9–11, we can see the harmonic spectrum of the source current in different working situations, and the THD was still under 5%, which means the system had strong robustness. In addition, the DC capacitor voltage tended to be stable by implementing the PI controller. It can be seen in Figure 12 that the DC capacitor voltage was also adjusted to a stable status regardless of the changes in the applied load.

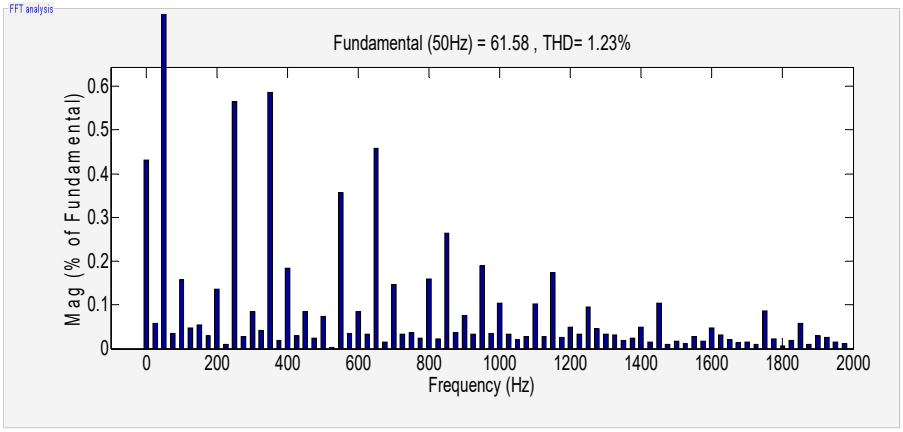


Figure 10. Harmonic spectrum of the source current at 0.16 s.

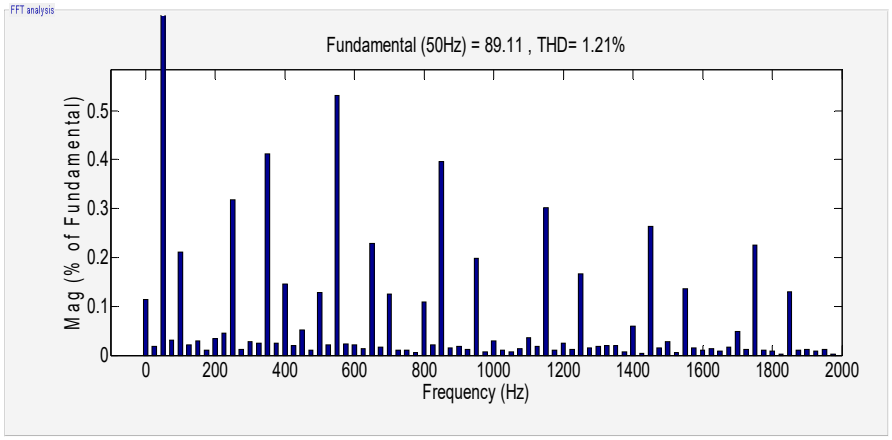


Figure 11. Harmonic spectrum of the source current at 0.26 s.

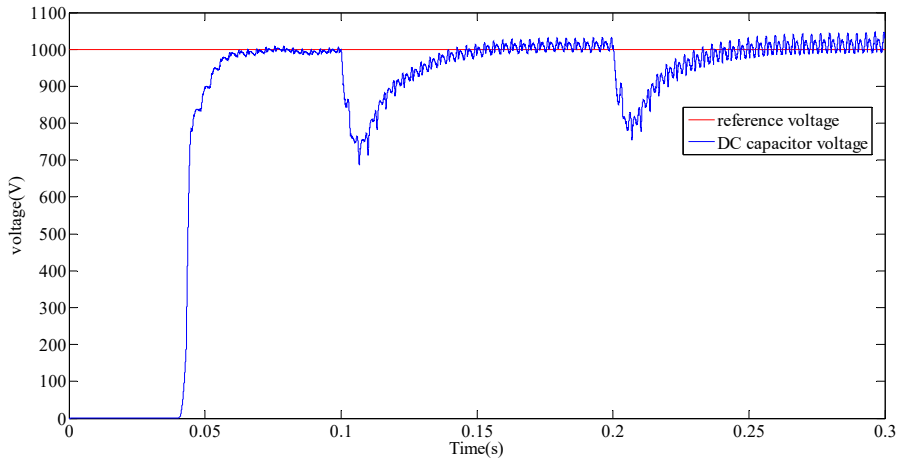
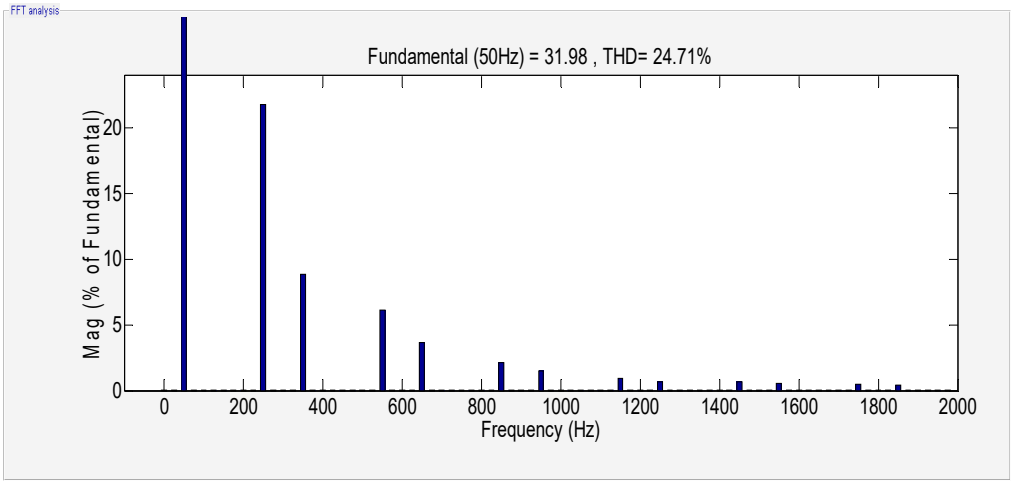


Figure 12. DC capacitor voltage with an increasing load.

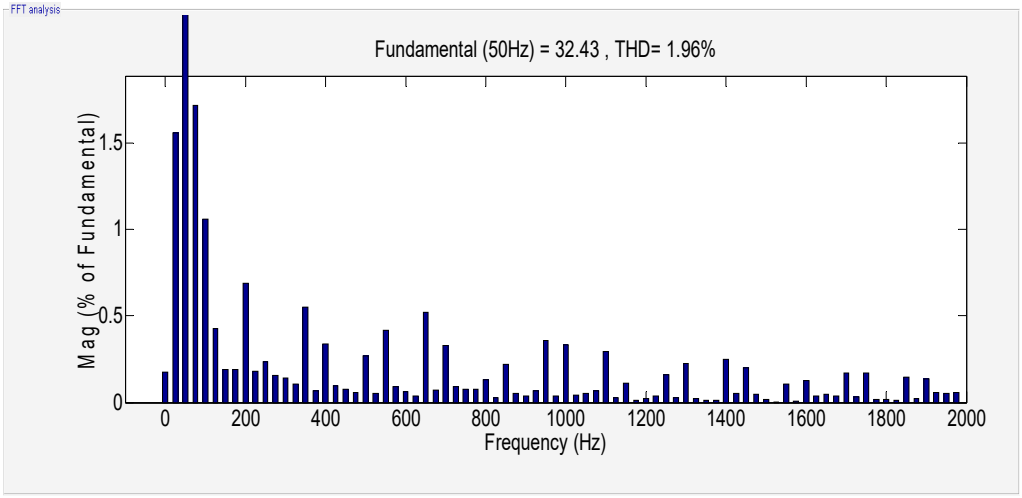
Finally, a comparison between the fuzzy sliding control system was also given so as to show the superiority of the proposed control. We can clearly see the better THD performance with the fractional control in Table 2. The performance of the APF was obviously better than that of the fuzzy sliding control method as shown in the THD values. The harmonic spectrum of fuzzy sliding mode control is shown in Figure 13.

Table 2. THD in the proposed controller and a normal controller.

Time	THD(%)	
	Fractional Sliding Mode Control	**Fuzzy Sliding Mode Control**
0	24.71%	24.71%
0.06 s	1.68%	1.96%
0.16 s	1.23%	1.49%
0.26 s	1.21%	1.44%

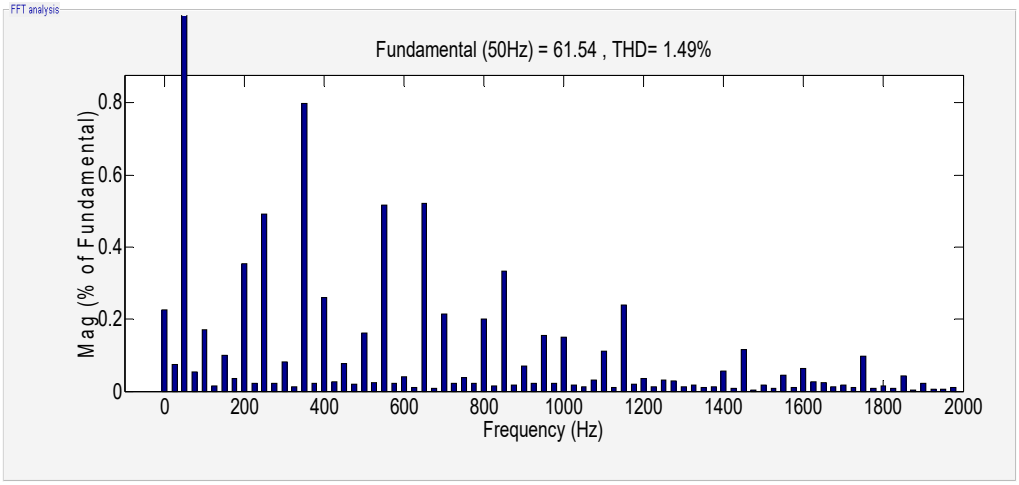


(**a**) 0 s

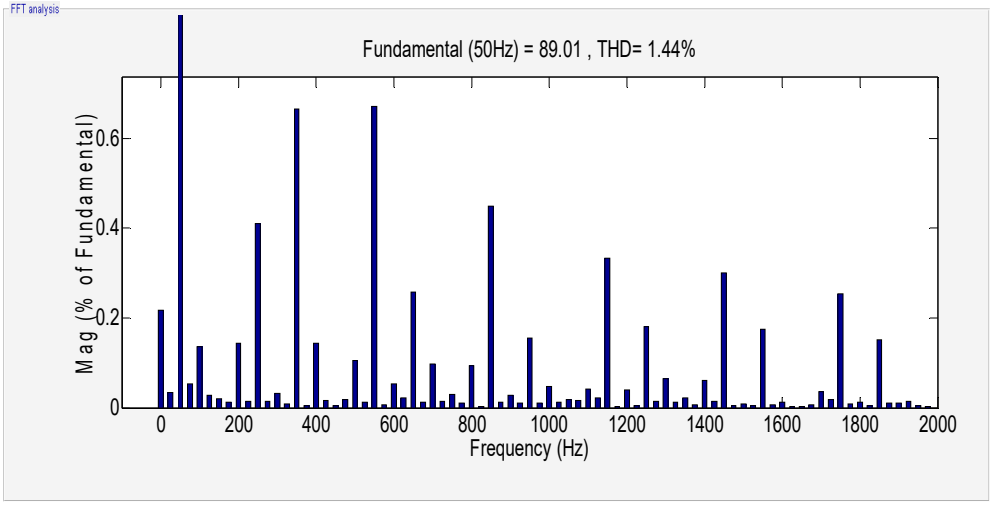


(**b**) 0.06 s

Figure 13. *Cont*.



(**c**) 0.16 s



(**d**) 0.26 s

Figure 13. Harmonic spectrum of the fuzzy sliding mode control at different times.

5. Conclusions

In this study, an FOSMC was developed and applied to a three-phase APF successfully. A fractional-order sliding mode surface was proposed, and the system was stable on the designed sliding surface. The SMC was combined with fractional-order control to have more degrees of freedom to obtain the desired performance. The proposed control system had the characteristics of a reduced tracking error and chattering. The simulation results with the comparison with the fuzzy sliding mode control confirmed the better compensation performance in the THD values with a 20% decrease.

Author Contributions: Conceptualization, W.F., M.H.; Validation, W.F.; Investigation, W.F.; Writing—original draft, W.F.; Writing—review & editing, M.H. All authors have read and agreed to the published version of the manuscript.

Funding: This research received no external funding.

Conflicts of Interest: The authors declare no conflict of interest.

References

1. Wu, Z.; Yang, Z.; Ding, K.; He, G. Order-Domain-Based Harmonic Injection Method for Multiple Speed Harmonics Suppression of PMSM. *IEEE Trans. Power Electron.* **2021**, *36*, 4478–4487. [CrossRef]
2. Jiao, N.; Wang, S.; Ma, J.; Chen, X.; Liu, T.; Zhou, D.; Yang, Y. The Closed-Loop Sideband Harmonic Suppression for CHB Inverter with Unbalanced Operation. *IEEE Trans. Power Electron.* **2021**, *37*, 5333–5341. [CrossRef]
3. Vahedi, H.; Shojaei, A.A.; Dessaint, L.-A.; Al-Haddad, K. Reduced DC-Link Voltage Active Power Filter Using Modified PUC5 Converter. *IEEE Trans. Power Electron.* **2017**, *33*, 943–947. [CrossRef]
4. Sun, X.; Han, R.; Shen, H.; Wang, B.; Lu, Z.; Chen, Z. A Double-Resistive Active Power Filter System to Attenuate Harmonic Voltages of a Radial Power Distribution Feeder. *IEEE Trans. Power Electron.* **2015**, *31*, 6203–6216. [CrossRef]
5. Rahmani, S.; Hamadi, A.; Al-Haddad, K.; Dessaint, L.A. A Combination of Shunt Hybrid Power Filter and Thyristor-Controlled Reactor for Power Quality. *IEEE Trans. Ind. Electron.* **2013**, *61*, 2152–2164. [CrossRef]
6. Tareen, W.U.K.; Mekhielf, S. Three-Phase Transformerless Shunt Active Power Filter with Reduced Switch Count for Harmonic Compensation in Grid-Connected Applications. *IEEE Trans. Power Electron.* **2018**, *33*, 4868–4881. [CrossRef]
7. Wai, R.; Yang, Z. Adaptive Fuzzy Neural Network Control Design via a T–S Fuzzy Model for a Robot Manipulator Including Actuator Dynamics. *IEEE Trans. Syst. Man Cybern. Part B Cybern.* **2008**, *38*, 1326–1346.
8. Liang, B.; Zheng, S.; Ahn, C.K.; Liu, F. Adaptive Fuzzy Control for Fractional-Order Interconnected Systems with Unknown Control Directions. *IEEE Trans. Fuzzy Syst.* **2020**, *30*, 75–87. [CrossRef]
9. Lu, J.; Savaghebi, M.; Ghias, A.M.Y.M.; Hou, X.; Guerrero, J.M. A Reduced-Order Generalized Proportional Integral Observer-Based Resonant Super-Twisting Sliding Mode Control for Grid-Connected Power Converters. *IEEE Trans. Ind. Electron.* **2020**, *68*, 5897–5908. [CrossRef]
10. Kumar, V.; Mohanty, S.R.; Kumar, S. Event Trigger Super Twisting Sliding Mode Control for DC Micro Grid with Matched/Unmatched Disturbance Observer. *IEEE Trans. Smart Grid* **2020**, *11*, 3837–3849. [CrossRef]
11. Zou, Z.-X.; Zhou, K.; Wang, Z.; Cheng, M. Frequency-Adaptive Fractional-Order Repetitive Control of Shunt Active Power Filters. *IEEE Trans. Ind. Electron.* **2014**, *62*, 1659–1668. [CrossRef]
12. Lin, H.; Guo, X.; Chen, D.; Wu, S.; Chen, G. A Frequency Adaptive Repetitive Control for Active Power Filter With 380V/75A SiC-Inverter. *IEEE Trans. Ind. Appl.* **2022**, *58*, 5469–5479. [CrossRef]
13. Navalkar, S.; Solingen, E.; Wingerden, J. Wind Tunnel Testing of Subspace Predictive Repetitive Control for Variable Pitch Wind Turbines. *IEEE Trans. Control. Syst. Technol.* **2015**, *23*, 2101–2116. [CrossRef]
14. Li, G.; Luo, A.; He, Z.; Ma, F.J.; Chen, Y.; Wu, W.; Zhu, Z.; Guerrero, J.M. A DC Hybrid Active Power Filter and Its Nonlinear Unified Controller Using Feedback Linearization. *IEEE Trans. Ind. Electron.* **2020**, *68*, 5788–5798. [CrossRef]
15. Hogan, D.J.; Gonzalez-Espin, F.J.; Hayes, J.G.; Lightbody, G.; Foley, R. An Adaptive Digital-Control Scheme for Improved Active Power Filtering Under Distorted Grid Conditions. *IEEE Trans. Ind. Electron.* **2017**, *65*, 988–999. [CrossRef]
16. Fei, J.; Liu, L. Real-Time Nonlinear Model Predictive Control of Active Power Filter Using Self-Feedback Recurrent Fuzzy Neural Network Estimator. *IEEE Trans. Ind. Electron.* **2021**, *69*, 8366–8376. [CrossRef]
17. Qi, W.; Liu, J.; Chen, X.; Christofides, P. Supervisory Predictive Control of Standalone Wind/Solar Energy Generation Systems. *IEEE Trans. Control. Syst. Technol.* **2011**, *19*, 199–207. [CrossRef]
18. Abry, X.; Sesmat, S.; Bideaux, É.; Ducat, C. Electropneumatic Cylinder Backstepping Position Controller Design With Real-Time Closed-Loop Stiffness and Damping Tuning. *IEEE Trans. Control. Syst. Technol.* **2016**, *24*, 541–552. [CrossRef]
19. Incremona, G.P.; Rubagotti, M.; Ferrara, A. Sliding Mode Control of Constrained Nonlinear Systems. *IEEE Trans. Autom. Control* **2016**, *62*, 2965–2972. [CrossRef]
20. Qu, L.; Qiao, W.; Qu, L. An Extended-State-Observer-Based Sliding-Mode Speed Control for Permanent-Magnet Synchronous Motors. *IEEE J. Emerg. Sel. Top. Power Electron.* **2021**, *9*, 1605–1613. [CrossRef]
21. Liu, H.; Wang, H.; Sun, J. Attitude control for QTR using exponential nonsingular terminal sliding mode control. *J. Syst. Eng. Electron.* **2019**, *30*, 191–200.
22. Chen, X.; Li, Y.; Ma, H.; Tang, H.; Xie, Y. A Novel Variable Exponential Discrete Time Sliding Mode Reaching Law. *IEEE Trans. Circuits Syst. II Express Briefs* **2021**, *68*, 2518–2522. [CrossRef]
23. Zhang, B.; Pi, Y.; Luo, Y. Fractional order sliding-mode control based on parameters auto-tuning for velocity control of permanent magnet synchronous motor. *ISA Trans.* **2012**, *51*, 649–656. [CrossRef]
24. Wang, J.; Zhou, Y.; Bao, Y.; Kim, H.; Lee, M. Trajectory Tracking Control Using Fractional-Order Terminal Sliding Mode Control with Sliding Perturbation Observer for a 7-DOF Robot Manipulator. *IEEE-ASME Trans. Mechatron.* **2020**, *25*, 1886–1893.
25. Kumar, V.; Ali, I. Fractional order sliding mode approach for chattering free direct power control of dc/ac converter. *IET Power Electron.* **2019**, *12*, 3600–3610. [CrossRef]
26. Ghasemi, S.; Tabesh, A.; Askari-Marnani, J. Application of Fractional Calculus Theory to Robust Controller Design for Wind Turbine Generators. *IEEE Trans. Energy Convers.* **2014**, *29*, 780–787. [CrossRef]

27. Cao, D.; Fei, J. Adaptive Fractional Fuzzy Sliding Mode Control for Three-Phase Active Power Filter. *IEEE Access* **2016**, mboxemph4, 6645–6651. [CrossRef]
28. Ullah, N.; Han, S. Adaptive fuzzy fractional-order sliding mode controller for a class of dynamical systems with uncertainty. *Trans. Inst. Meas. Control.* **2016**, *38*, 402–413. [CrossRef]

Disclaimer/Publisher's Note: The statements, opinions and data contained in all publications are solely those of the individual author(s) and contributor(s) and not of MDPI and/or the editor(s). MDPI and/or the editor(s) disclaim responsibility for any injury to people or property resulting from any ideas, methods, instructions or products referred to in the content.